

PET versus SPECT: strengths, limitations and challenges

Arman Rahmim^a and Habib Zaidi^b

The recent introduction of high-resolution molecular imaging technology is considered by many experts as a major breakthrough that will potentially lead to a revolutionary paradigm shift in health care and revolutionize clinical practice. This paper intends to balance the capabilities of the two major molecular imaging modalities used in nuclear medicine, namely positron emission tomography (PET) and single photon emission computed tomography (SPECT). The motivations are many-fold: (1) to gain a better understanding of the strengths and limitations of the two imaging modalities in the context of recent and ongoing developments in hardware and software design; (2) to emphasize that certain issues, historically and commonly thought as limitations of one technology, may now instead be viewed as challenges that can be addressed; (3) to point out that current state of the art PET and SPECT scanners can (greatly) benefit from improvements in innovative image reconstruction algorithms; and (4) to identify important areas of research in PET and SPECT imaging that will be

instrumental to further improvements in the two modalities. Both technologies are poised to advance molecular imaging and have a direct impact on clinical and research practice to influence the future of molecular medicine. *Nucl Med Commun* 29:193–207 © 2008 Wolters Kluwer Health | Lippincott Williams & Wilkins.

Nuclear Medicine Communications 2008, 29:193–207

Keywords: molecular imaging, PET, SPECT, sensitivity, spatial resolution, temporal resolution

^aDepartment of Radiology, Johns Hopkins Medical Institutions, Baltimore, Maryland, USA and ^bDivision of Nuclear Medicine, Geneva University Hospital, Geneva, Switzerland

Correspondence to Dr Habib Zaidi, Division of Nuclear Medicine, Geneva University Hospital, CH-1211 Geneva 4, Switzerland
Tel: +41 22 372 7258; fax: +41 22 372 7169;
e-mail: habib.zaidi@hcuge.ch

Received 7 September 2007 Accepted 13 October 2007

Introduction

This paper intends to balance, in the context of recent and ongoing developments, the capabilities of the two major molecular imaging modalities in nuclear medicine, namely positron emission tomography (PET) and single photon emission computed tomography (SPECT). Comparison of the two imaging modalities in terms of molecular biology is presented elsewhere [1,2], and except for very brief comments, this review focuses on the physics of molecular imaging (hardware and software aspects). At first glance, it may be thought that the targeting abilities (and therefore biological aspects) of different compounds in PET versus SPECT are the only issues to consider in order to select which to use in each context. Certainly, biological considerations are the ultimate deciding factors when comparing PET vs. SPECT. It is also worth noting that in the biological context, generalized comparisons are not appropriate; instead they need to be performed on a case-by-case basis. For instance, it is often argued that the natural occurrence of PET isotopes in biologically active molecules (as opposed to heavy isotopes used in SPECT) results in a less challenging task of synthesizing physiologically useful tracers in PET. On the other hand, in some applications, SPECT agents can provide more specific targeting abilities than PET agents. However, such an isolated approach, in which physical capabilities of the two modalities are neglected, is bound to result in

(costly) flawed conclusions and misleading statements [3,4].

The importance of physical considerations can be better seen, for example, in the case of cardiac PET vs. SPECT. Coronary perfusion and myocardial viability are most commonly performed with SPECT. While SPECT has many applications in neurology and oncology, the majority of SPECT scans are performed in the field of cardiology. SPECT is now a cornerstone with any patient with heart disease. At the same time, some published results suggest that PET may offer increased accuracy and improved sensitivity compared to SPECT [5,6], particularly for heavier patients, where breast, chest wall and diaphragmatic attenuation interfere with conventional SPECT. One of the reasons is that attenuation correction is easily achieved in PET, whereas it is (often) not implemented accurately in SPECT [7]. However, latest trends in SPECT imaging attempt to accurately address attenuation correction (see attenuation correction section), and therefore the latest generation of SPECT cameras (or improved software for current SPECT cameras) should be able to produce improved performance [8].

In this paper, the first three sections compare capabilities in PET and SPECT in terms of sensitivity, spatial resolution and temporal resolution, respectively. Various ongoing developments aiming at enhancing the

performance of PET and SPECT modalities are discussed, both in terms of optimal hardware design (e.g., slit/slat, slant-hole and pinhole collimators) and software development (e.g., finite resolution modelling and compensation, dynamic image reconstruction). Complications related to attenuation correction (especially in SPECT) and random coincidences (in PET) are addressed in the next, two sections. Finally, time-of-flight detection (unique to PET) and dual-tracer imaging (still clinically unique to SPECT but might be feasible for PET in the future) are emphasized in the subsequent three sections, respectively, as additional areas of research and development. The following section discusses other data correction techniques (scatter, partial volume and motion corrections) necessary for obtaining quantitatively accurate images. Concluding remarks and future directions are presented in the last section of this paper.

Sensitivity

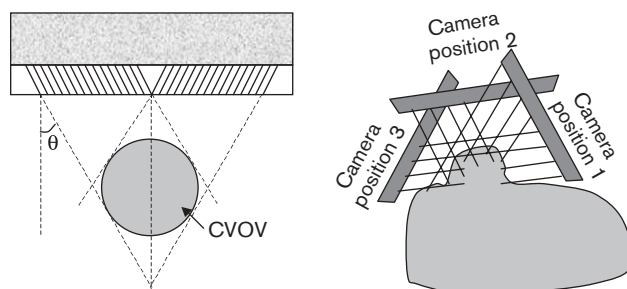
The most important advantage of PET imaging over SPECT is that of exhibiting a much higher sensitivity (by approximately two to three orders of magnitude); i.e., the ability to detect and record a higher percentage of the emitted events, which has very important implications (see coincident detection in PET subsection). This is because, in single-photon imaging (planar and SPECT), physical collimators are needed in order to reject photons that are not within a small angular range (otherwise the angle of incidence will not be known). Collimators therefore exhibit low geometric efficiencies (defined as the percentage of detected to emitted photon), of the order of $\sim 0.01\%$.

On the other hand, SPECT offers the possibility to widen the observational time window (owing to the longer half-life of single photon emitters) thus allowing biomedical scientists to observe biological processes *in vivo* several hours or days after administration of the labelled compound [9].

SPECT collimators

In SPECT, a number of approaches were investigated to increase sensitivity through optimal design of the collimator. One approach is to use shorter collimators in order to reject a smaller portion of incident events. However, this approach degrades the resolution of the camera (the well-known 'sensitivity versus resolution' trade-off). On the other hand, novel types of collimator (as opposed to conventional parallel-hole collimators) have been able to improve sensitivity without adversely affecting resolution. It must be noted that the task of tomography is performed differently for each collimators design, and therefore specifically designed reconstruction algorithms need to be implemented. Important examples of these include (1) rotating slat collimators [10–13], (2) converging-hole (e.g., fan-beam and cone-beam) collima-

Fig. 1



A two-segment slant-hole collimator (left). Parallel holes within each segment are slanted towards a common volume of view (CVOV) where the organ to be imaged is placed. The slant-angle, θ , is shown. Three camera stops, equally spaced around the organ (for $\theta=30^\circ$, only 120° needs to be covered), while the collimator rotates at each camera stop (right).

tors [14,15], and (3) rotating multi-segment slant-hole (RMSSH) collimators [16,17], among many other designs [18–20]. The first method uses the idea of rotating parallel slats, with the intrinsic advantage of slats (instead of holes) having a much larger solid angle of acceptance. The second and third methods, instead, gain in sensitivity by means of scanning a smaller field of view (FoV). Pinhole collimators with only one or a few channels have been designed to image small organs and human extremities in addition to small animals [21] and are further discussed in the SPECT subsection.

Particularly interesting are RMSSH collimators (Fig. 1) because in addition to improving the scanner sensitivity by a factor of ~ 2 or ~ 4 (depending on whether two or four segments are used), they can achieve *complete* angle tomography, with as few as $180^\circ/(2\theta)$ camera positions, where θ is the slant angle (e.g., only three camera positions when $\theta=30^\circ$, which corresponds to a single camera stop for a triple-head scanner) assuming sufficient collimator rotation-sampling is performed at the camera positions [16,17]. Furthermore, the amount of camera rotation needed is $180^\circ-2\theta$ (i.e., less than 180°) making it very convenient for SPECT mammography [22] since the camera can be placed closer to the breast (making it suitable for detecting small, low-contrast breast lesions). This is also shown in Fig. 1. A newer variation involving collimator holes that are slanted at variable angles to form a planar diverging-beam geometry has also been suggested involving a larger FoV though with minimum decrease in detection efficiency [23].

Coincidence detection in PET

Due to the nature of positron annihilation in which two opposite annihilation photons are emitted from the same event, physical collimators can be entirely removed in

PET, with the collimation instead performed electronically using the coincidence-detection method. This implies a much larger angle of acceptance at each detector position, resulting in the order of $\sim 1\%$ of emitted events being detected in PET.

There are a number of important implications to this significant gain in sensitivity for PET:

- (1) *Improved image quality* Owing primarily to the random (Poisson) nature of radioactive decay, noise is an inherent component of nuclear medicine imaging. For multiple measurements, the percentage noise (ratio of standard deviation, σ , to the average, m , of the total counts detected in a certain time interval) along a projection is given by:

$$\% \text{ noise} = \frac{\sigma}{m} = \frac{1}{\sqrt{m}} \quad (1)$$

given that $\sigma = \sqrt{m}$ when dealing with Poisson statistics. Improvements in sensitivity (i.e., increasing m) therefore improve signal-to-noise ratios (SNRs) in the data, which also corresponds to improvements in image SNR (see Strigl *et al.* [24] and Stearns [25,26] for details of methods relating data SNR to image SNR).

- (2) *Possibility of performing shorter scans* An increase in sensitivity implies the ability to acquire shorter scans with similar SNRs.
- (3) *Multiple field-of-view scanning* The ability to perform shorter scans also implies the feasibility of performing multiple scans of a patient at different fields of view in a reasonable time. This is a very important consideration in clinical oncology.
- (4) *Improved temporal resolution* As will be elaborated in Temporal resolution section, higher sensitivity of PET scanners implies an increased ability to acquire shorter (and therefore a higher number of) frames in dynamic studies, resulting in an improved ability to study dynamic biological processes.

It must be noted that the technique of coincidence detection used in PET, while highly improving sensitivity, introduces two issues which have been subjects of further investigation: (1) non-collinearity of annihilation photons (see Finite resolution effects in PET section) and (2) detection of random coincidences (see Temporal resolution section).

Effect of short half-lives in PET

In the present context, an additional observation is that the short half-lives of radionuclides used in PET effectively allow for increased detection sensitivity over a given period of time. This is because compared to SPECT imaging, radiotracers with shorter half-lives can be injected in *higher* activities to the patient without

posing any additional radiation damage to the patient (since overall accumulation over time remains the same) thus generating increased detectable radiation over a shorter time.

An example of this, with much recent interest, is rubidium (^{82}Rb)-based PET [27]. Because rubidium has a very short physical half-life of only 76 s, it can be injected in very high (yet safe) amounts (e.g., 2 GBq) allowing for acceptable images in very short times. Compared to routine SPECT myocardial stress imaging, which can take place over 3–4 h (this time can be potentially halved using simultaneous dual-tracer imaging as elaborated in sections on dual-tracer imaging in both SPECT and PET), a complete pharmacological stress-and-rest test may instead be performed in well under 1 h in ^{82}Rb -based cardiac PET (considerably increasing patient comfort as well as number of daily patient scans). In addition, the almost instantaneous ability of rubidium to image a patient has provided a very high accuracy in identification of ischaemia [28].

Spatial resolution

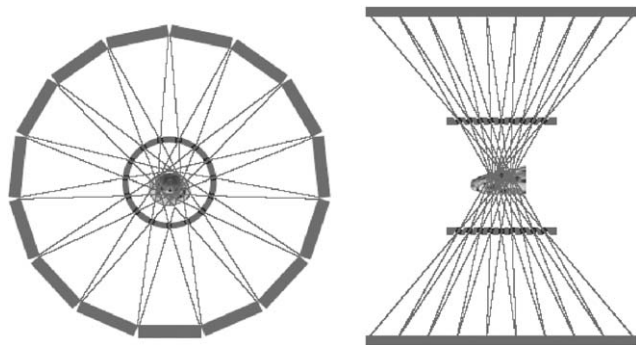
Spatial resolution performance in PET and SPECT is related to a number of different factors. A general observation is that improvements in SPECT resolution are effectively only limited by *technology* (e.g., collimator design), whereas in PET imaging, two *physics*-related limitations, namely positron range and photon non-collinearity, ultimately limit system resolution (it must be noted, however, that, as discussed later, these effects can be modelled in the reconstruction task, as opposed to simply being treated as resolution-limiting, therefore further improving reconstructed resolutions) [29]. Related issues are discussed next.

Pinhole SPECT

Pinhole SPECT is an exciting example of technological advance which has introduced the possibility of considerably enhancing image resolution in SPECT (to sub-millimetre scale), particularly in the context of small animal imaging [30]. However, it must be noted that use of a small pinhole further decreases system sensitivity. Subsequently, *multi*-pinhole collimators have been proposed and implemented [21].

A complicating factor with the high-resolution pinhole approach is the task of calibrating the SPECT devices (especially in the presence of camera rotations). An innovative solution to this consideration, which at the same time noticeably increases system sensitivity, is the design of *stationary* dedicated pinhole SPECT systems making use of a large number of compact detectors with multiple pinhole geometries. An example of such design is the U-SPECT-I system [31,32] containing 75 pinholes, as shown in Fig. 2. Therefore, stationary

Fig. 2



The design of U-SPECT-I contains a total of 75 gold pinhole apertures: 15 pinholes in each ring (left) with a total of nine rings (right). Not shown here is that pinhole positions in adjacent rings are rotated transaxially with respect to each other by 8° in order to increase the variety of angles at which each voxel is observed. Reprinted with permission from Beekman and Vastenhouw [31].

multi-pinhole SPECT imaging using dedicated detectors provides a combination (and *not* trade-off) of high resolution and high sensitivity, and furthermore, considerably enhances possibilities of dynamic imaging. However, one may add that these systems would still likely require axial translation schemes since they cover a very limited FoV.

Finite resolution effects in SPECT

In SPECT, the image generated from a point source is degraded by a number of factors related to collimators and detectors in gamma cameras, thus referred to as the collimator–detector response (CDR). Therefore, for any particular SPECT camera, the CDR can be a measure of the image resolution; however, this is valid only if no further compensation is included. In recent years, a great deal of work has gone into developing methods to compensate for the CDR [33].

The CDR is determined by the following four factors:

- (1) *Intrinsic response* Aside from the effect of collimators, the detector system itself demonstrates an intrinsic uncertainty in position estimation of incident gamma rays. This is caused by two factors: (a) the statistical signal variation (noise) in signal output of PMTs used for position estimation, and (b) change/spread in signal energy deposition in the detector due to scattering (especially for higher energy isotopes, e.g., ^{111}In).
- (2) *Geometric response* Collimator dimensions define the acceptance angle within which incident photons are accepted. Subsequently, the geometric response function becomes wider with increasing distance from the collimator surface, and strongly depends on the particular design of each collimator.

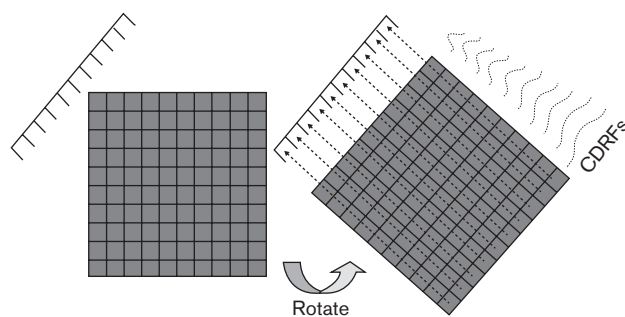
- (3) *Septal penetration* The CDR is further degraded owing to the penetration of some photons through the collimator septa. No analytical treatment of this effect appears to exist in the literature, and Monte Carlo simulation techniques have been used instead (e.g., Cot *et al.* [34], Du *et al.* [35] and Staelens *et al.* [36]).
- (4) *Septal scatter* This effect is caused by photons that scatter in the collimator septa and still remain within the detection energy window. Similar to septal penetration, this effect may also be computed using Monte Carlo simulation techniques.

Analytical methods taking into account the distance dependence of the CDR function (CDRF) have been proposed in the literature (see Frey and Tsui [37] for a review of both related analytical and statistical methods). However, compared to statistical methods, analytical methods suffer from (1) a general lack of ability to treat statistical noise in the data, and (2) making specific approximations, for instance with regards to the shape and/or distance dependence of the CDRF, in order to arrive at analytical solutions.

With the increasing realization of the power of statistical methods in nuclear medicine, and particularly with the development of convenient and fast rotation-based projectors in SPECT [38–40], as shown in Fig. 3, iterative reconstruction methods incorporating distance-dependent CDRFs are increasing in popularity. The use of Gaussian diffusion methods [41,42] can further increase the speed of rotation-based projectors.

Incorporation of CDR modelling in reconstruction algorithms (especially statistical methods) has been shown to result in improvements in spatial resolution [41], noise

Fig. 3



Rotation-based projector methods incorporating distant-dependent CDRFs make use of the fact that, for parallel-beam geometries, the CDRF is spatially invariant in rows (planes) parallel to the collimator face. Thus, each row (plane) may be convolved with the appropriate distance-dependent CDRF.

[43], and more importantly in *task-based* measures of image-quality: e.g., improved uniformity in the myocardial wall as well as improved estimates of wall thickness [44], improved myocardial defect detection using both simulated [45,46] and clinical data [47], as well as improved performance for tumour detection and localization [48].

Finite resolution effects in PET

In PET imaging, three factors contribute to degradation of resolution in the reconstructed images: detector-related effects, photon non-collinearity and positron range. Detector-related effects (which in PET are due to (1) the width of scintillation crystals, (2) inter-crystal scattering, and (3) inter-crystal penetration) are continually improving with advances in technology and algorithmic developments, and similar to CDR compensation in SPECT, may be modelled in the reconstruction task to further improve reconstructed resolution [49,50] (the recent high definition ‘HD-PET’ development introduced by Siemens Medical Solutions relies on this kind of improved system modelling to deliver outstanding improvements in image quality [51]). In what follows, we elaborate the remaining two inherent resolution-degrading factors in PET: photon non-collinearity and positron range.

Photon non-collinearity

Since the net momentum for an emitted positron, and the electron with which it annihilates, can be non-zero, this results in deviations from 180° between the trajectories of the two emitted photons (due to conservation of momentum) as shown in Fig. 4 [52,53]. This deviation is around 0.25° FWHM, and the corresponding resolution blurring depends on detector separation (or ring diameter), D , and is approximately given by:

$$\text{FWHM} \approx \left(0.25 \times \frac{\pi}{180}\right) \frac{D}{2} \quad (2)$$

That is,

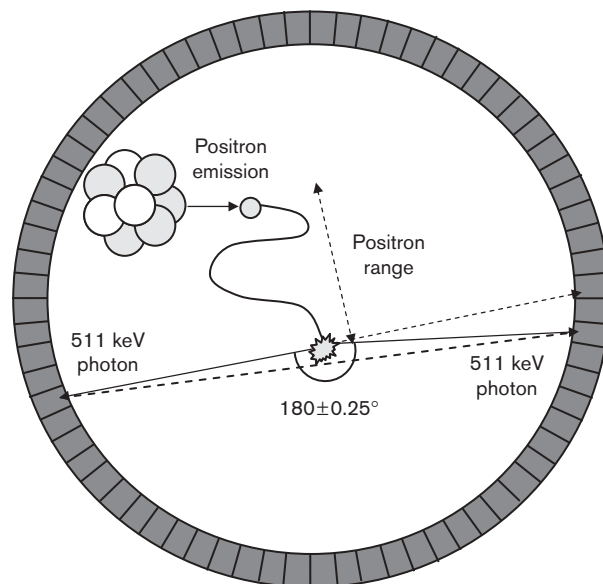
$$\text{FWHM} \approx 0.0022 \times D \quad (3)$$

Therefore one expects ~ 1.54 – 1.76 mm FWHM blurring for a typical whole-body scanner ($D \sim 70$ – 80 cm), whereas this blurring may be much reduced for animal scanners (e.g., only 0.17 mm for $D \sim 8$ cm). A more extensive analysis of the effect of annihilation photons non-collinearity and depth of interaction on spatial resolution in PET are given by Sanchez-Crespo and Larsson [54].

Positron range

Emitted positrons travel a certain distance, on average, in the surrounding medium before they can reach thermal energies in order to be annihilated. This distance is referred to as the positron range (Fig. 4). Different

Fig. 4



Depiction of the finite positron range and the non-collinearity of the annihilation photons inherent to the positron–electron annihilation process which give rise to an inherent positional inaccuracy not present on conventional SPECT. Positron range and angle are to a great extent exaggerated; distribution of angles around 180° is Gaussian, with a standard deviation equal to 0.25° .

positron-emitting isotopes exhibit distinct energy distributions, and therefore also exhibit different positron range values. An extensive analysis of positron range distributions for different materials and their impact on the spatial resolution of PET scanners is given by Shibuya *et al.* [53], Levin and Hoffman [55], Sanchez-Crespo *et al.* [56] and Palmer *et al.* [57].

Traditionally, positron range has been viewed as a purely resolution-limiting factor. However, there are two additional approaches (one hardware-based and the other software-based) that can be used to reduce this effect.

Effect of magnetic fields Simulations [58,59] as well as experiments [60,61] have verified the possibility of improving PET scanner resolution by application of a strong magnetic field, which is known to reduce the positron range. It must be noted that this effect is most significant: (1) at field strengths of ~ 5 T or more; (2) for high-energy positron-emitting radionuclides, e.g., ^{68}Ga and ^{82}Rb . This is one of the advantages of designing PET detectors compatible with MRI/NMR systems. However, there are many other more important motivations for implementation of such combined/simultaneous systems including: (1) to reduce inaccuracies of registration between functional and anatomical images (e.g., avoiding problems of subject movement and any deformation of

organs in-between scans); (2) to perform functional MRI (fMRI) and PET in exactly the same environment (e.g., for cross-validation); and (3) similarly to provide temporal correlation for PET and NMR spectroscopy as a potentially very powerful technique [62,63]. Furthermore, patient motion may be potentially monitored using MRI, and subsequently incorporated into PET image reconstruction. If successfully implemented in clinical environments, this technology might replace combined PET/CT in the future [64,65].

However, when employing lower-energy positron-emitting radionuclides such as ^{18}F or ^{11}C , simulations/experiments with typical human PET scanners (resolutions of ~ 3 mm or higher) have indicated that improvements in resolution will not to be significant [59,61]. For such radionuclides, this effect may only become noticeable for small animal scanners and remains to be demonstrated. The reason is that, in addition to having smaller detectors, the effect of photon non-collinearity is also small in animal PET scanners (see Equation 3), and therefore reductions in positron range will more readily affect overall scanner resolution.

Modelling into the reconstruction task Positron range (and photon non-collinearity) are conventionally not discussed as physical phenomenon that can be corrected for; rather, they are often seen as limitations of PET imaging. However, with the arrival of statistical reconstruction algorithms (and the concept of the system matrix) [29,66], even though it is not possible to determine these effects for each particular detected event, it is possible to calculate and incorporate their probability distributions into the system matrix [67]. Such advanced modelling in turn can result in improvements in image resolution. It has also been suggested that this can improve the noise properties [68,69], as also shown in the case of incorporating collimator-detector response modelling in SPECT [43] (see Finite resolution effects in SPECT section).

Results of improvements in PET technology

From the above observations, it is evident that improvements in PET technology as well as reconstruction algorithms will continue to yield further improvements in high-resolution PET imaging. Much worthwhile research efforts have been carried out in this field, particularly in the context of small animal PET imaging [70], resulting in reconstructed volumetric resolutions reaching $\sim 1\ \mu\text{l}$ (e.g., microPET Focus scanner [71]). As a last note, a very promising ongoing technological development is the use of avalanche photodiodes (APDs) whose compactness compared to bulky photomultiplier tubes (PMTs) offers new opportunities in high-resolution imaging (in addition to their high quantum efficiency, internal gain and insensitivity to magnetic fields, as well as the potential of these silicon-based detectors to be ultimately made

very cheaply in high volumes) [62,72,73]. On the other hand, silicon photomultipliers (SiPMs), a finely pixelated APD operated in 'Geiger mode', became commercially available in the last 3 years [74] from several manufacturers such as Photonique (a distributor for CPTA, Russia), Hamamatsu (Japan) or SensL (Ireland). In contrast to APDs, this light readout technology presents a high signal amplification owing to their high internal gain combined with low noise behaviour. Even though current systems consist of first prototypes and it is potentially several years before cheap mass production is reachable, SiPMs are very promising candidates for use as photodetectors in PET and, especially, PET/MR [75].

Temporal resolution

The ability to perform dynamic imaging in nuclear medicine is becoming increasingly important. This is because, in many cases, it is the change in the bio-distribution of radiopharmaceuticals within the body that offers the most information about the underlying physiological processes. This, in turn, brings in the concept of temporal resolution: how frequently (over a period of time) an imaging instrument is able to capture 'acceptable' images of an object in the FoV. Compared to spatial resolution, it is more difficult to precisely quantify temporal resolution. This depends on specifying what may or may not be considered as an 'acceptable' image of sufficient quality. The criteria of sufficient image quality are specific to the particular imaging task.

It must be noted that the temporal resolution has a dependence on the reconstruction algorithm being used. For instance, as noted in spatial resolution section, the use of advanced statistical reconstruction algorithms, e.g., modelling positron range (in PET) or collimator-detector response (in SPECT), can improve image quality (e.g., both spatial resolution and signal-to-noise ratios), thus improving the temporal resolution. As noted in Coincidence detection in PET section, the temporal resolution is also very closely related to the sensitivity of the imaging system. In this sense, PET imaging has an intrinsic advantage over SPECT for dynamic studies.

Dynamic SPECT

In SPECT (without having assumptions about image dynamics), it is necessary to perform complete angle tomography via camera rotations for each dynamic frame, which limits how fast each frame may be acquired (an exception to this is stationary multi-pinhole SPECT used in animal imaging, as discussed in Pinhole SPECT section, which does not involve camera rotations, though it covers a limited FoV). Even when using very fast rotation acquisitions (down to even 5 s per rotation with a three-head camera), the acquisitions at each position will provide very low statistics.

An alternative approach in SPECT is to perform slow camera rotations (e.g., a single rotation for the entire study) while making assumptions about image dynamics. For instance, in fatty acid myocardial viability studies, it has been assumed that the activity $\lambda_j(t)$ of the j -th position (voxel) of the heart at time t may be modelled as:

$$\lambda_j(t) = A_j \exp(-a_j t) + B_j \exp(-b_j t) + C_j \quad (4)$$

where the above-mentioned approach would involve estimating the five kinetic parameters A_j , B_j , C_j , a_j and b_j directly from the measured data [76] (also consult Kadmas and Gullberg [77] for a list of references using this type of approach).

Other investigators [78,79] have instead approached this problem without making strict assumptions about the functional behaviour of the tracer over time (i.e., unlike Equation 4) and instead have made the minimal assumption that the activity at each voxel j does not increase with time. A more flexible scenario is considered by Farncombe *et al.* [80] in which organ uptake (i.e., increasing activity) is allowed at the beginning. While such methods provide less restriction, the problem with not making implicit kinetic model assumptions can be shown in the following example. For a typical image slice of size 64×64 reconstructed into 16 dynamic frames from data acquired over 64 projections (each with 64 bins), this last approach requires using 64×64 measurements to estimate $16 \times 64 \times 64$ unknowns (i.e., activity of each voxel at each frame), which is highly underestimated. On the other hand, using the direct parameter estimation model above (e.g., Equation 4 which contains five parameters to be estimated for each voxel), $5 \times 64 \times 64$ unknowns need to be estimated.

An alternative, more natural approach to dynamic SPECT involves the use of 4-D maximum *a posteriori* (MAP) reconstruction algorithms in which the behaviour of each voxel in time is encouraged to conform to a compartmental model [77]. In the above-referenced work, the kinetic parameters are updated after every iteration of the reconstruction algorithm. A good review of MAP regularization can be found in Qi and Leahy [66]. The interested reader may also consult Rahmim *et al.* [81] for detailed discussion of 4-D MAP image reconstructions. It must be noted, that this reference discusses the different context of 4-D reconstruction of cardiac/respiratory-gated data. In such a context, 4-D MAP approaches are used to encourage the behaviour of each voxel to conform to the measured or modelled cardiac/respiratory motion.

Dynamic PET

Dynamic PET imaging does not encounter the above-mentioned complications with dynamic SPECT. A general approach to dynamic PET imaging consists of independently reconstructing tomographic data obtained within each dynamic frame (e.g., Rahmim *et al.* [82]).

Nevertheless, recent work has indicated that the availability of a list-mode acquisition capability in modern PET scanners in which the time of detection for each event is also stored can be used to further improve temporal resolution. This is because conventional dynamic PET reconstruction methods assume the activity to be constant within each frame. Instead, new approaches make use of temporal basis functions to allow the activity in each voxel to be represented continuously over time [83–85]. Next, the coefficients of the basis functions are estimated making collective use of the entire dataset and the individual times of arrival for each event (this is an example of 4-D PET reconstruction).

Another interesting application of PET is in dynamic cardiac imaging. As an example, ^{13}N -labelled ammonia ($^{13}\text{NH}_3$) can be used for the measurement of myocardial blood flow which makes it possible to measure blood flow at the level of micro-circulation. At the same time, measurement of myocardial wall motion can be used to assess the global function of the heart through the ejection fraction. These tasks can be performed by introduction of dynamic frames each of which is cardiac gated (which has the additional advantage of reducing cardiac motion artefacts). It is worth noting that in this context, temporal resolution may be further improved by truly 5-D [3-D (spatial information) + 1-D (time) + 1-D (ECG signal)] reconstruction algorithms which make use of the list-mode data and continuous temporal representation of activities in the voxels, across the frames and the gates [86].

Attenuation correction

Photon attenuation refers to the property of emitted radiation to interact with tissue and other materials as it passes through the body. For photon energies encountered in nuclear medicine (68–80 keV for ^{201}Tl to 511 keV for positron emitters), photons can undergo photoelectric interactions (though negligible at 511 keV) as well as scattering. Mathematically, the surviving probability of radiation (i.e., not being attenuated) along a path L through an attenuating object can be expressed as:

$$P_L = \exp \left[- \int_L \mu(x) d\vec{x} \right] \quad (5)$$

where P_L is the survival probability; the parameter μ is referred to as the linear attenuation coefficient, which is an energy- and tissue-dependent measure of photon attenuation; and \vec{x} is the line along which the line of response (LOR) is located and thus along which the μ integral is taken.

The critical observation is that in PET, the path length, L , represents the line of response (LOR) along which the dually emitted photons travel, and therefore attenuation

is *independent* of the point of origin along the LOR, whereas in SPECT, due to its single-photon emission nature, attenuation changes depending on the point of emission. The task of attenuation correction in PET is therefore more straightforward. A number of approaches have been proposed [7], most common of which include incorporation of the measured attenuation factors for each LOR as (1) pre-correction factors in the measured data or as (2) multiplicative factors inside the system matrix of the image reconstruction task.

What we wish to emphasize in this section is that attenuation correction in SPECT is not a limitation, rather it is simply more challenging to address. In the past, due to weak hardware/software implementations (as well as a desire to minimize time and expense costs), attenuation correction has not been widely performed in SPECT. However, the importance of attenuation correction in SPECT is becoming increasingly realized [87–89]. Since the thickness of tissue varies for different regions of the patient's anatomy, errors introduced by lack of attenuation correction will also vary regionally (e.g., a lesion located deep within the body will produce a more highly attenuated signal compared to a superficial lesion; also, for instance, in myocardial perfusion imaging, soft-tissue attenuation due to the diaphragm or breast tissue can cause false positive defects). As such, it has become widely accepted that artefact-free, quantitatively accurate SPECT imaging may only be performed by including attenuation correction in the long chain of data processing techniques. The introduction of SPECT/CT scanners has served as a convenient and fast solution to measurement of the transmission data using X-rays [90]. However, effects such as respiratory-induced misregistration of the emission and transmission data [91–95], truncation artefacts owing to discrepancy between fields of view in a dual-modality system [96–99], the presence of oral and intravenous contrast medium [100–110], artefacts due to metallic implants [111–117], beam-hardening artefacts caused by the polychromatic nature of CT X-rays [118,119], X-ray scatter in CT images for future generation cone-beam geometries [120–122], and other CT artefacts from any source, need to be carefully considered.

In the past, for applications employing attenuation correction in SPECT, the 'multiplicative Chang technique' [123] (as well as its iterative versions) had been mostly used; however, these techniques are based on the assumption of uniformly attenuating medium. On the other hand, statistical reconstruction algorithms have a special ability to model (and compensate) for the presence of uniform or non-uniform attenuation in the detection process (e.g., the attenuated projector-back-projector pair as described by Gullberg *et al.* [124]). With the increasing realization of the importance [43] and convenience of compensation for both the CDR function

as well as non-uniform attenuation (particularly using convenient rotation-based projectors [38–40] as elaborated in Finite resolution effects in SPECT section), the incorporation of attenuation compensation in statistical reconstruction methods are finally moving towards wide acceptance by the SPECT community [7].

Random coincidences in PET

The technique of coincidence detection used in PET has a complication (not present in SPECT) in that two annihilation photons that are detected/accepted within the same coincidence timing window, may not have originated from the same event. The direct consequence is that an incorrect LOR is assigned to two simultaneous annihilation photons whose pairs, for example, exit the scanner undetected. Alternatively, the other pairs could also have not been detected due to being scattered out of the field of view (i.e., attenuated) or simply passed through the scanner undetected (detectors are not 100% efficient). Mathematically, the rate of random coincidences along such an LOR connecting two detectors i and j is given by:

$$R = 2\tau S_i S_j \quad (6)$$

where τ is the coincidence timing window, and S_i and S_j refer to the singles rates at the two detectors.

Correction for random coincidences (*randoms*) is the subject of ongoing research in PET imaging. Rahmim *et al.* [82] have included an elaborate review of relevant techniques (particularly in the context of statistical image reconstruction). The conventional approach has been to subtract a (noisy, Poisson distributed) estimate of the randoms (obtained using the delayed-coincidence technique) from the measured coincidences. There are, however, two issues with this approach: (1) even though this approach corrects for randoms on the average, it increases the noise in the data; (2) data corrected in this way are no longer Poisson distributed (a subtraction of Poisson variables results in a variable that is no longer Poisson distributed unlike addition), while most existing statistical image reconstruction algorithms assume Poisson distribution of the data [125].

Alternatively, to avoid the above two issues, it is possible to follow an approach in which an averaged (i.e., non-noisy) estimate of the random rates along each LOR are included in the image reconstruction task [82]. The random rates estimates, required in this approach, can be calculated using (1) singles measurements at the detectors [126] to calculate the expected randoms contribution according to Equation 6, or (2) variance reduction (smoothing) of the measured noisy (delayed coincidence) estimates of randoms [127–129].

Defining T and R as the number of true and random coincidences detected in a scan, and using

Poisson-statistics arguments (while neglecting scattered events), it can be shown that the SNR in the data is given by:

$$SNR = \frac{T}{\sqrt{T + 2R}} \quad (7)$$

when using a delayed-coincidence subtraction technique, while it improves (increases) to:

$$SNR = \frac{T}{\sqrt{T + R}} \quad (8)$$

when using the alternative approaches discussed above. Considering Equation 8, we note that while in PET, random rates are of the same approximate order as the true rates $R \sim T$, in SPECT random coincidences do not exist ($R = 0$); however, since $T(\text{PET}) \gg T(\text{SPECT})$, it follows that SNRs are still considerably greater in PET compared to SPECT imaging [130].

It must further be noted that the development of fast (and at the same time high light output) scintillators such as lutetium oxyorthosilicate (LSO) and lutetium yttrium oxyorthosilicate (LYSO) and LaBr_3 have allowed the coincidence timing window τ to be noticeably reduced (2–4 ns) compared to typical values (~ 10 – 12 ns) achieved with conventional bismuth germanate (BGO) scanners [131,132]. Considering Equation 6, this improvement can be seen to reduce the random rates, and thus to further improve count-rate performance of PET scanners (as a side note: LSO, in fact, has the potential of exhibiting a timing FWHM resolution of < 0.5 ns, which is a very important consideration in time-of-flight PET; see Time-of-flight detection in PET section).

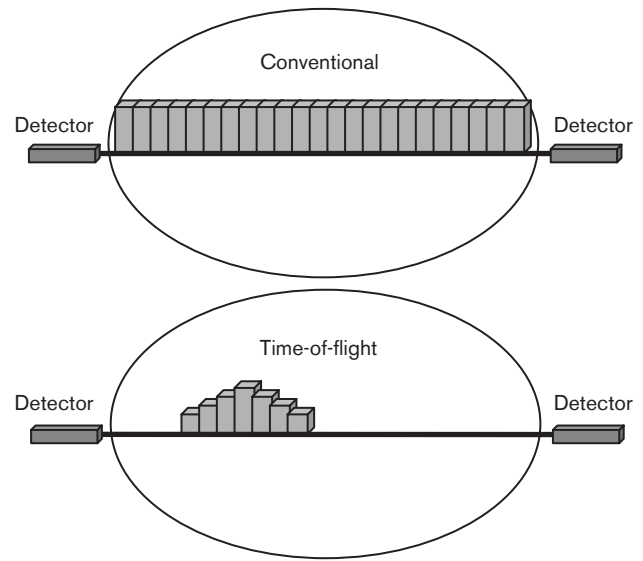
Therefore, as a final note in this section, consideration of fast scintillators in PET, as well as careful estimations of random coincidences and their inclusion in appropriate image reconstruction algorithms can result in successful removal of bias in the images while also minimizing degradation/noise amplification in the PET data.

Time-of-flight detection in PET

An additional improvement in the quality of PET images may be made making use of the dual nature of emitted annihilation photons. Time-of-flight (ToF) PET is based on the observation that by measuring the difference of the arrival times of the 511 keV photons, a PET camera could restrict the position of the positron emission to a subsection of the line segment joining the detector pair. This is shown in Fig. 5.

It had been known since the early 1980s that PET scanners capable of encoding ToF information would potentially reduce the statistical noise variance in PET reconstruction [133,134]. However, technological difficulties (slow electronics and the need for fast and at the

Fig. 5



With conventional reconstruction (top) voxels along the LOR are incremented regardless of position along the LOR. With TOF reconstruction (bottom), each voxel is incremented by the probability (as measured by the TOF measurement) that the source originated at that voxel.

same time effectively absorbing scintillators), had limited development of ToF PET until recently. With the continuous improvements in the technology of PET imaging (e.g., faster electronics), and especially since the discovery of the scintillator LSO, ToF PET was recently actively reconsidered [132,135,136] leading to the development of the first commercial scanner by one manufacturer [137].

ToF PET, especially in whole-body scanning, has been shown to considerably improve image noise behaviour compared to conventional schemes in which ToF information is not incorporated. The reduction factor, f , in the noise variance for a ToF system capable of a timing resolution of Δt is given by [132]:

$$f \approx \frac{2D}{c\Delta t} \quad (9)$$

where D is the size of the emission source, and c is the speed of light. The elegant study by Conti [138] should be consulted for a more detailed consideration of the effects of random coincidences and scattered events). In fact, optimum Δt values down to ~ 300 ps and ~ 200 ps have been measured for LSO and LaBr_3 , both of which are very promising candidates for ToF PET. For a realistic Δt of ~ 500 ps (expected for next-generation LSO-based scanners), the noise variance improvements will correspond to factors of ~ 4.7 in whole-body ($D \sim 35$ cm) and ~ 2.7 in brain ($D \sim 20$ cm) imaging.

Dual-tracer SPECT imaging

Simultaneous dual-tracer imaging using SPECT is an area of increasing interest. The dual-tracer approach is difficult to perform in PET imaging due to all its radiotracers being of the same energy (511 keV) level (see following section), whereas multiple-energy windows can be used in SPECT for simultaneous imaging of radiotracers of different energies.

Examples of this include: (1) ^{99m}Tc (140 keV) sestamibi stress and ^{201}Tl (75 keV/167 keV) rest myocardial perfusion imaging, and (2) simultaneous use of a ^{99m}Tc (140 keV) labelled perfusion agent and an ^{123}I (159 keV) labelled neurotransmitter agent (with potential applications in diagnosis of neurodegenerative diseases, e.g., Parkinson's, Huntington's and Alzheimer's diseases).

The use of simultaneous acquisition reduces acquisition times and therefore patient discomfort and image artefacts due to patient motion. Another significant advantage is that the resulting images from the different tracers are perfectly registered in space and time.

A complication with dual-tracer imaging is the presence of crosstalk between the multiple energy windows. In the case of, for instance, imaging with ^{99m}Tc (140 keV) and ^{201}Tl (75 keV/167 keV), the lower-energy ^{201}Tl energy window is contaminated by ^{99m}Tc photons scattered in the patient or collimator (referred to as down-scatter) as well as Pb X-rays generated by both scattered and unscattered ^{99m}Tc photons in the collimator. In addition, the ^{99m}Tc data are also contaminated by scattered (~ 135 keV) and unscattered (167 keV) ^{201}Tl photons.

To address the above difficulties, current research has focussed on optimization of multiple energy-window acquisition parameters [139,140] as well as modelling of cross-talk effects (i.e., down-scatter and collimator X-ray generation) in the reconstruction task [141–143]. Combinations of these methods as well as detailed clinical evaluation are still required in order to make dual-tracer SPECT imaging an acceptable clinical protocol.

Feasibility of dual-tracer PET imaging

Simultaneous dual-tracer imaging is extremely difficult to perform and is still in its infancy. The feasibility of fast scanning of multiple PET tracers using dynamic imaging techniques, where the signals from each tracer are separated based upon differences in tracer half-life, kinetics, and distribution has been investigated by Kadmas and Rust in a well-designed study [144,145]. The single-tracer components can then be assessed through multivariate analysis tools such as principal component analysis (PCA). The preliminary results obtained using dynamic dual-tracer imaging with staggered injections appear to allow recovering overlapping

signals through the use of information from kinetics and radioactive decay. In a follow-up study, the same group demonstrated that blood flow quantification can be achieved in only 20 min by the fast dual-tracer approach with accuracy similar to that of conventional separate rest and stress scans [146]. This field is now an area of active research [147,148] and to be successful, the approach deserves further research and development efforts and additional evaluation for potential clinical use.

Another potential application of rapid dual-tracer PET imaging would be to exploit its advantages to construct a patient-specific attenuation map on transmissionless PET scanning devices including combined PET/MR [64]. A combination of fluoride (^{18}F) PET for bone scanning with the tracer of interest (e.g., ^{11}C -methionine) should allow scanning both tracers in a single acquisition. The bone scan could be used for accurate determination of the distribution of bony structures within the patient thus allowing to derive a non-uniform attenuation map in whole-body PET/MR studies.

Other data corrections

In order to produce fully quantitative data, three other corrections need to be considered. The reader is referred elsewhere for elaborate reviews of these topics [81,149–151]; here we briefly compare their applications in PET versus SPECT.

Scatter correction

Scatter correction is one of the most important and at the same time most difficult corrections in nuclear medicine imaging. Scattered events can constitute 30–50% of all events in SPECT, 10–20% in 2-D PET and 40–60% in 3-D PET. The difficulty in scatter compensation is due to the fact that, in order to truly estimate the number of scattered events along each projection, the emission image needs to be known, which is the very aim of the reconstruction task. The reader is referred to Zaidi and Koral [149] for a thorough review of the various approaches.

An approach of increasing interest is the use of fast analytical [152–156] or Monte Carlo [157–160] based scatter calculations inside iterative reconstruction algorithms, such that the scatter estimate is updated at every step. However, it must be noted that due to the comparatively greater sizes of data in PET, most of the research performed in this field is related to SPECT imaging. Compression schemes are being developed to make the technique feasible even on high-resolution PET systems with large axial field of view [161].

Correction for partial volume effect

The partial volume effect (PVE) arises due to the limited spatial resolution in nuclear medicine imaging (and is

relevant for 'small' regions with dimensions smaller than around two to three times the FWHM of the scanner resolution). It has been shown to result in large biases in the estimates of regional radioactivity concentrations. The reader is referred to Soret *et al.* [150] and Rousset *et al.* [151] for an elaborate review of this topic. The methods developed in this area are equally applicable in both PET and SPECT imaging, and require, for best performance, access to anatomical images (CT or MRI) of the subjects.

Motion compensation

The majority of motion-compensation methods (image-based and projection-based) are equally applicable in both PET and SPECT [162]. These have been reviewed, for rigid, cardiac and respiratory motions, in Rahmim *et al.* [81]. There are, however, two potential differences between the two modalities in the context of motion compensation: (1) in SPECT, there exists a correlation between projection angle and time (therefore motion); this time dependence may be potentially used in the motion compensation task [163]; and (2) the enormous size of PET data can cause difficulties for demanding motion compensation methods. Subsequently, accurate and at the same time fast methods are needed in PET (see Rahmim *et al.* [81] for details).

Conclusions and future directions

The present paper has attempted to summarize important themes of ongoing hardware and software advancements for the two major imaging modalities in molecular imaging. In the context of PET imaging, the coincidence-detection method is viewed as a very powerful method, considerably enhancing sensitivity and dynamic-imaging capabilities of PET. Furthermore, use of very short half-life tracers (e.g., ^{82}Rb) injected at very high activities, as well as the introduction of increasingly fast scintillators technology (particularly for LSO), which in turn has allowed reduction of random coincidences and introduced the possibility of time-of-flight PET are expected to further contribute to high-sensitivity imaging capabilities of PET. Improvements in PET technology (e.g., detector design), modelling of finite resolution effects in PET image reconstruction, as well as the potential of applying magnetic fields on simultaneous PET/MR systems (expected to reduce positron range for high-energy positron-emitting radionuclides) are also seen as areas of ongoing research attempting to improve resolution limitations in PET.

In SPECT, the use of specialized collimators (e.g., slant-hole) is viewed as a technique for improving sensitivity without degrading image resolution. Furthermore, pin-hole SPECT technology is seen as an area of intense recent interest, particularly due to its ability to enhance resolution capabilities in SPECT (to sub-millimetre

range) and to offer the possibility of stationary small animal SPECT imaging. Incorporation of non-uniform attenuation in SPECT as well as collimator-detector response and scatter modelling into statistical iterative image reconstruction algorithms was also seen as an area of considerable potential towards artefact-free, quantitative SPECT imaging. Various issues related to temporal resolution (and dynamic imaging capabilities) in SPECT and PET were also discussed. In particular, it was seen that use of suitable (4-D and 5-D) reconstruction algorithms could further enhance temporal resolution capabilities of these imaging modalities. Finally, it should be stressed that existing PET and SPECT technologies in the field can (greatly) benefit from improvements in image reconstruction software, and from the potential of dual-tracer imaging as well as the use of specialized collimators in the case of SPECT.

An important issue related to dual-modality imaging is worth mentioning when putting SPECT and PET modalities into perspective. PET/CT has received wide clinical acceptance and already had a valuable outcome on clinical oncology practice and cancer treatment. This has encouraged scanner manufacturers to replace standalone PET scanners with combined PET/CT units. Although the number of installed SPECT/CT systems continues to increase at a healthy pace, the evolution of SPECT/CT did not follow the same trend. One of the main reasons for the slow acceptance of SPECT/CT compared to PET/CT is the relative cost of SPECT and CT taking into account the low fraction of clinical indications where SPECT/CT is needed [164].

Given that the role of any molecular imaging technology is established with respect to benefits conveyed to patients, SPECT and PET will definitely maintain an exclusive standing in clinical diagnosis, assessment of response to treatment and delivery of targeted therapies, but their superior picomolar sensitivity is being challenged by competing technologies, such as those using ultra-small superparamagnetic contrast agents.

Acknowledgement

This work was supported by the Swiss National Science Foundation under grant SNSF 3152A0-102143.

References

- 1 Cherry S. *In vivo* molecular and genomic imaging: new challenges for imaging physics. *Phys Med Biol* 2004; **49**:R13–R48.
- 2 Fullerton GD, Hazle JD. The development of technologies for molecular imaging should be driven principally by biological questions to be addressed rather than by simply modifying existing imaging technologies. For the proposition. *Med Phys* 2005; **32**:1231–1233.
- 3 Maisey M. Is PET the future of nuclear medicine? *Eur J Nucl Med Mol Imaging* 2003; **30**:1045–1046.
- 4 Bailey DL. Is PET the future of nuclear medicine? *Eur J Nucl Med Mol Imaging* 2003; **30**:1047–1049.
- 5 Segall G. Assessment of myocardial viability by positron emission tomography. *Nucl Med Commun* 2002; **23**:323–330.

- 6 Di Carli MF, Hachamovitch R. Should PET replace SPECT for evaluating CAD? The end of the beginning. *J Nucl Cardiol* 2006; **13**:2–7.
- 7 Zaidi H, Hasegawa B. Attenuation correction strategies in emission tomography. In: Zaidi H, editor: *Quantitative Analysis in Nuclear Medicine Imaging*. New York: Springer; 2006. pp. 167–204.
- 8 Madsen MT. Recent advances in SPECT imaging. *J Nucl Med* 2007; **48**:661–673.
- 9 Meikle SR, Kench P, Kassiou M, Banati RB. Small animal SPECT and its place in the matrix of molecular imaging technologies. *Phys Med Biol* 2005; **50**:R45–R61.
- 10 Lodge MA, Webb S, Flower MA, Binnie DM. A prototype rotating slat collimator for single photon emission computed tomography. *IEEE Trans Med Imaging* 1996; **15**:500–511.
- 11 Gagnon D, Zeng GL, Links JM, Griesmer JJ, Valentino FC. Design considerations for a new solid-state gamma-camera: SOLSTICE. *Proc IEEE Nuclear Science Symposium and Medical Imaging Conference* 2001; **2**:1156–1160.
- 12 Zeng GL, Gagnon D. Image reconstruction algorithm for a spinning strip CZT SPECT camera with a parallel slat collimator and small pixels. *Med Phys* 2004; **31**:3461–3473.
- 13 Vandenberghe S, Van Holen R, Staelens S, Lemahieu I. System characteristics of SPECT with a slat collimated strip detector. *Phys Med Biol* 2006; **51**:391–405.
- 14 Jaszczak RJ, Greer KL, Coleman RE. SPECT using a specially designed cone beam collimator. *J Nucl Med* 1988; **29**:1398–1405.
- 15 Tsui BM, Gullberg GT. The geometric transfer function for cone and fan beam collimators. *Phys Med Biol* 1990; **35**:81–93.
- 16 Clack R, Christian PE, Defrise M, Welch AE. Image reconstruction for a novel SPECT system with rotating slant-hole collimators. *IEEE Conference Record Nuclear Science Symposium and Medical Imaging Conference* 1994; **4**:1948–1952.
- 17 Wagner JM, Noo F, Clackdoyle R. Exact inversion of the exponential x-ray transform for rotating slant-hole (RSH) SPECT. *Phys Med Biol* 2002; **47**:2713–2726.
- 18 Kimiaei S, Ljungberg M, Larsson SA. Evaluation of optimally designed planar-concave collimators in single-photon emission tomography. *Eur J Nucl Med* 1997; **24**:1398–1404.
- 19 Beekman FJ, Kamphuis C, Hutton BF, van Rijk PP. Half-fanbeam collimators combined with scanning point sources for simultaneous emission-transmission imaging. *J Nucl Med* 1998; **39**:1996–2003.
- 20 Formiconi AR. Geometrical response of multihole collimators. *Phys Med Biol* 1998; **43**:3359–3379.
- 21 Beekman F, van der Have F. The pinhole: gateway to ultra-high-resolution three-dimensional radionuclide imaging. *Eur J Nuc Med Mol Imaging* 2007; **34**:151–161.
- 22 Brzymialkiewicz CN, Tornai MP, McKinley RL, Bowshe JE. Evaluation of fully 3-D emission mammotomography with a compact cadmium zinc telluride detector. *IEEE Trans Med Imaging* 2005; **24**:868–877.
- 23 Liu C, Xu J, Tsui B. Development and evaluation of rotating multi-segment variable-angle slant-hole SPECT [Abstract]. *J Nucl Med* 2007; **48**:161P.
- 24 Strigl M, Martinez M-J, Zach C, Ziegler SI, Hahn K. Performance evaluation of the PET sub-systems of two PET/CT imagers according to NEMA standard NU 2-2001. *Z Med Phys* 2006; **16**:83–91.
- 25 Stearns C. Estimating an acquisition-specific NEC curve for PET acquisitions. *Records IEEE Nuclear Science Symposium and Medical Imaging Conference* 2003; **4**:2578–2580.
- 26 Stearns C. NEC and local image noise in PET imaging. *Records IEEE Nuclear Science Symposium and Medical Imaging Conference* 2004; **5**:3106–3108.
- 27 Di Carli MF, Dorbala S, Meserve J, El Fakhri G, Sitek A, Moore SC. Clinical myocardial perfusion PET/CT. *J Nucl Med* 2007; **48**:783–793.
- 28 Jadvar H, Strauss HW, Segall GM. SPECT and PET in the evaluation of coronary artery disease. *Radiographics* 1999; **19**:915–926.
- 29 Reader A, Zaidi H. Advances in PET image reconstruction. *PET Clinics* 2007; **2**:(in press).
- 30 Weber DA, Ivanovic M. Ultra-high-resolution imaging of small animals: implications for preclinical and research studies. *J Nucl Cardiol* 1999; **6**:332–344.
- 31 Beekman FJ, Vastenhouw B. Design and simulation of a high-resolution stationary SPECT system for small animals. *Phys Med Biol* 2004; **49**:4579–4592.
- 32 Vastenhouw B, Beekman F. Submillimeter total-body murine imaging with U-SPECT-I. *J Nucl Med* 2007; **48**:487–493.
- 33 Frey EC, Tsui BM, Gullberg GT. Improved estimation of the detector response function for converging beam collimators. *Phys Med Biol* 1998; **43**:941–950.
- 34 Cot A, Sempau J, Pareto D, Bullich S, Pavia J, Calvino F, et al. Evaluation of the geometric, scatter, and septal penetration components in fan-beam collimators using Monte Carlo simulation. *IEEE Trans Nucl Sci* 2002; **49**:12–16.
- 35 Du Y, Frey EC, Wang WT, Tocharoenchai C, Baird WH, Tsui BMW. Combination of MCNP and SimSET for Monte Carlo simulation of SPECT with medium- and high-energy photons. *IEEE Trans Nucl Sci* 2002; **49**:668–674.
- 36 Staelens S, de Wit T, Beekman F. Fast hybrid SPECT simulation including efficient septal penetration modelling (SP-PSF). *Phys Med Biol* 2007; **52**:3027–3043.
- 37 Frey E, Tsui B. Collimator-detector response compensation in SPECT. In: Zaidi H, editor: *Quantitative Analysis of Nuclear Medicine Images*. New York: Springer; 2006. pp. 141–166.
- 38 McCarthy AW, Miller MI. Maximum-likelihood SPECT in clinical computation times using mesh-connected parallel computers. *IEEE Trans Med Imaging* 1991; **10**:426–436.
- 39 Zeng GL, Gullberg GT. Frequency domain implementation of the three-dimensional geometric point source correction in SPECT imaging. *IEEE Trans Nucl Sci* 1992; **39**:1444–1453.
- 40 Feng B, Gifford HC, Beach RD, Boening G, Gennert MA, King MA. Use of three-dimensional Gaussian interpolation in the projector/backprojector pair of iterative reconstruction for compensation of known rigid-body motion in SPECT. *IEEE Trans Med Imaging* 2006; **25**:838–844.
- 41 Kohli V, King MA, Glick SJ, Pan TS. Comparison of frequency-distance relationship and Gaussian-diffusion-based methods of compensation for distance-dependent spatial resolution in SPECT imaging. *Phys Med Biol* 1998; **43**:1025–1037.
- 42 Beekman FJ, Slijpen ETP, Niessen WJ. Supervised diffusion parameter selection for filtering SPECT brain images. *Scale-Space Theory Comput Vis* 1997; **1252**:164–175.
- 43 Tsui BM, Frey EC, Zhao X, Lalush DS, Johnston RE, McCartney WH. The importance and implementation of accurate 3D compensation methods for quantitative SPECT. *Phys Med Biol* 1994; **39**:509–530.
- 44 Kohli V, King MA, Pan T-S, Glick SJ. Compensation for distance-dependent resolution in cardiac-perfusion SPECT: impact on uniformity of wall counts and wall thickness. *IEEE Trans Nucl Sci* 1998; **45**:1104–1110.
- 45 Sankaran S, Frey EC, Gilland KL, Tsui BM. Optimum compensation method and filter cutoff frequency in myocardial SPECT: a human observer study. *J Nucl Med* 2002; **43**:432–438.
- 46 Frey EC, Gilland KL, Tsui BMW. Application of task-based measures of image quality to optimization and evaluation of three-dimensional reconstruction-based compensation methods in myocardial perfusion SPECT. *IEEE Trans Med Imaging* 2002; **21**:1040–1050.
- 47 Narayanan MV, King MA, Pretorius PH, Dahlberg ST, Spencer F, Simon E, et al. Human-observer receiver-operating-characteristic evaluation of attenuation, scatter, and resolution compensation strategies for Tc-99m myocardial perfusion imaging. *J Nucl Med* 2003; **44**:1725–1734.
- 48 Gifford HC, King MA, Wells RG, Hawkins WG, Narayanan MV, Pretorius PH. LROC analysis of detector-response compensation in SPECT. *IEEE Trans Med Imaging* 2000; **19**:463–473.
- 49 Mumcuoglu EU, Leahy RM, Cherry SR, Hoffman E. Accurate geometric and physical response modelling for statistical image reconstruction in high resolution PET. *Conference Record IEEE Nuclear Science Symposium* 1996; **3**:1569–1573.
- 50 Selivanov VV, Picard Y, Cadorette J, Rodrigue S, Lecomte R. Detector response models for statistical iterative image reconstruction in high resolution PET. *IEEE Trans Nucl Sci* 2000; **47**:1168–1175.
- 51 Panin VY, Kehren F, Michel C, Casey M. Fully 3-D PET reconstruction with system matrix derived from point source measurements. *IEEE Trans Med Imaging* 2006; **25**:907–921.
- 52 Iwata K, Greaves RG, Surko CM. Gamma-ray spectra from positron annihilation on atoms and molecules. *Phys Rev A* 1997; **55**:3586–3604.
- 53 Shibuya K, Yoshida E, Nishikido F, Suzuki T, Tsuda T, Inadama N, et al. Annihilation photon acollinearity in PET: volunteer and phantom FDG studies. *Phys Med Biol* 2007; **52**:5249–5261.
- 54 Sanchez-Crespo A, Larsson SA. The influence of photon depth of interaction and non-collinear spread of annihilation photons on PET image spatial resolution. *Eur J Nucl Med Mol Imaging* 2006; **33**:940–947.
- 55 Levin CS, Hoffman EJ. Calculation of positron range and its effect on the fundamental limit of positron emission tomography system spatial resolution. *Phys Med Biol* 1999; **44**:781–799. Corrigendum: *Phys Med Biol* 2000; **45**:559.
- 56 Sanchez-Crespo A, Andreo P, Larsson SA. Positron flight in human tissues and its influence on PET image spatial resolution. *Eur J Nucl Med Mol Imaging* 2004; **31**:44–51.

- 57 Palmer MR, Zhu X, Parker JA. Modeling and simulation of positron range effects for high resolution PET imaging. *IEEE Trans Nucl Sci* 2005; **52**:1391–1395.
- 58 Hammer BE, Christensen NL, Heil BG. Use of a magnetic field to increase the spatial resolution of positron emission tomography. *Med Phys* 1994; **21**:1917–1920.
- 59 Raylman RR, Hammer BE, Christensen NL. Combined MRI-PET scanner: a Monte-Carlo evaluation of the improvements in PET resolution due to the effects of a static homogeneous magnetic field. *IEEE Trans Nucl Sci* 1996; **43**:2406–2412.
- 60 Christensen NL, Hammer BE, Heil BG, Fetterly K. Positron emission tomography within a magnetic field using photomultiplier tubes and light-guides. *Phys Med Biol* 1995; **40**:691–697.
- 61 Wirrwar A, Vosberg H, Herzog H, Halling H, Weber S, Muller-Gartner H-W. 4.5 tesla magnetic field reduces range of high-energy positrons – potential implications for positron emission tomography. *IEEE Trans Nucl Sci* 1997; **44**:184–189.
- 62 Pichler BJ, Judenhofer MS, Catana C, Walton JH, Kneilling M, Nutt RE, et al. Performance test of an LSO-APD detector in a 7-T MRI scanner for simultaneous PET/MRI. *J Nucl Med* 2006; **47**:639–647.
- 63 Cherry SR. The 2006 Henry N. Wagner lecture: Of mice and men (and positrons) – Advances in PET imaging technology. *J Nucl Med* 2006; **47**:1735–1745.
- 64 Zaidi H. Is MRI-guided attenuation correction a viable option for dual-modality PET/MR imaging? *Radiology* 2007; **242**:639–642.
- 65 Zaidi H, Mawlawi O, Orton CG. Point/counterpoint. Simultaneous PET/MR will replace PET/CT as the molecular multimodality imaging platform of choice. *Med Phys* 2007; **34**:1525–1528.
- 66 Qi J, Leahy RM. Iterative reconstruction techniques in emission computed tomography. *Phys Med Biol* 2006; **51**:R541–R578.
- 67 Reader AJ, Ally S, Bakatselos F, Manavaki R, Walledge R, Jeavons AP, et al. One-pass list-mode EM algorithm for high-resolution 3-D PET image reconstruction into large arrays. *IEEE Trans Nucl Sci* 2002; **49**:693–699.
- 68 Rafecas M, Boning G, Pichler BJ, Lorenz E, Schwaiger M, Ziegler SI. Effect of noise in the probability matrix used for statistical reconstruction of PET data. *IEEE Trans Nucl Sci* 2004; **51**:149–156.
- 69 Rahmim A, Cheng J-C, Sossi V. Improved noise propagation in statistical image reconstruction with resolution modeling. *IEEE Nuclear Science Symposium Conference Record* 2005; **5**:2576–2578.
- 70 Tai YC, Laforest R. Instrumentation aspects of animal PET. *Annu Rev Biomed Eng* 2005; **7**:255–285.
- 71 Tai YC, Ruangma A, Rowland D, Siegel S, Newport DF, Chow PL, et al. Performance evaluation of the microPET focus: a third-generation microPET scanner dedicated to animal imaging. *J Nucl Med* 2005; **46**:455–463.
- 72 Shah KS, Grazioso R, Farrell R, Glodo J, McClish M, Entine G, et al. Position sensitive APDs for small animal PET imaging. *IEEE Trans Nucl Sci* 2004; **51**:91–95.
- 73 Dumouchel T, Bergeron M, Cadorette J, Lepage M, Selivanov V, Lapointe D, et al. Initial performance assessment of the LabPET™ APD-based digital PET scanner [Abstract]. *J Nucl Med* 2007; **48**:39P.
- 74 Dolgoshein B, Balagura V, Buzhan P, Danilov M, Filatov L, Garutti E, et al. Status report on silicon photomultiplier development and its applications. *Nucl Instrum Meth A* 2006; **563**:368–376.
- 75 Moehrs S, Del Guerra A, Herbert DJ, Mandelkern MA. A detector head design for small-animal PET with silicon photomultipliers (SiPM). *Phys Med Biol* 2006; **51**:1113–1127.
- 76 Limber M, Limber M, Celler A, Barney J, Borwein J. Direct reconstruction of functional parameters for dynamic SPECT. *IEEE Trans Nucl Sci* 1995; **42**:1249–1256.
- 77 Kadrmas DJ, Gullberg GT. 4D maximum a posteriori reconstruction in dynamic SPECT using a compartmental model-based prior. *Phys Med Biol* 2001; **46**:1553–1574.
- 78 Farncombe T, Celler A, Noll D, Maight J, Harrop R. Dynamic SPECT imaging using a single camera rotation (dSPECT). *IEEE Trans Nucl Sci* 1999; **46**:1055–1061.
- 79 Bauschke H, Dominikus N, Celler A. An EM Algorithm for dynamic SPECT. *IEEE Trans Med Imaging* 1999; **18**:252–261.
- 80 Farncombe T, Celler A, Bever C, Noll D, Maight J, Harrop R. The incorporation of organ uptake into dynamic SPECT (dSPECT) image reconstruction. *IEEE Trans Nucl Sci* 2001; **48**:3–9.
- 81 Rahmim A, Rousset OG, Zaidi H. Strategies for motion tracking and correction in PET. *PET Clinics* 2007; **2**:(in press).
- 82 Rahmim A, Cheng J-C, Blinder S, Camborde M-L, Sossi V. Statistical dynamic image reconstruction in state-of-the-art high-resolution PET. *Phys Med Biol* 2005; **50**:4887–4912.
- 83 Nichols TE, Qi J, Asma E, Leahy RM. Spatiotemporal reconstruction of list-mode PET data. *IEEE Trans Med Imaging* 2002; **21**:396–404.
- 84 Reader AJ, Sureau FC, Comtat C, Trebossen R, Buvat I. Joint estimation of dynamic PET images and temporal basis functions using fully 4D ML-EM. *Phys Med Biol* 2006; **51**:5455–5474.
- 85 Verhaeghe J, D'Asseler Y, Staelens S, Lemahieu I. Optimization of temporal basis functions in dynamic PET imaging. *Nucl Instr Meth A* 2006; **569**:425–428.
- 86 Verhaeghe J, D'Asseler Y, Staelens S, Vandenberghe S, Lemahieu I. Reconstruction for gated dynamic cardiac PET imaging using a tensor product spline basis. *IEEE Trans Nucl Sci* 2007; **54**:80–91.
- 87 Wackers FJT. Should SPET attenuation correction be more widely employed in routine clinical practice? Against. *Eur J Nucl Med* 2002; **29**:412–415.
- 88 Ficaro EP. Should SPET attenuation correction be more widely employed in routine clinical practice? For. *Eur J Nucl Med* 2002; **29**:409–412.
- 89 Heller GV, Links J, Bateman TM, Ziffer JA, Ficaro E, Cohen MC, et al. American Society of Nuclear Cardiology and Society of Nuclear Medicine joint position statement: attenuation correction of myocardial perfusion SPECT scintigraphy. *J Nucl Cardiol* 2004; **11**:229–230.
- 90 Blankespoor SC, Xu X, Kaiki K, Brown JK, Tang HR, Cann CE, et al. Attenuation correction of SPECT using X-ray CT on an emission–transmission CT system: myocardial perfusion assessment. *IEEE Trans Nucl Sci* 1996; **43**:2263–2274.
- 91 Goerres GW, Burger C, Kamel E, Seifert B, Kaim AH, Buck A, et al. Respiration-induced attenuation artifact at PET/CT: Technical considerations. *Radiology* 2003; **226**:906–910.
- 92 Osman MM, Cohade C, Nakamoto Y, Wahl RL. Respiratory motion artifacts on PET emission images obtained using CT attenuation correction on PET-CT. *Eur J Nucl Med Mol Imaging* 2003; **30**:603–606.
- 93 Papathanassiou D, Becker S, Amir R, Meneroux B, Liehn JC. Respiratory motion artefact in the liver dome on FDG PET/CT: comparison of attenuation correction with CT and a caesium external source. *Eur J Nucl Med Mol Imaging* 2005; **32**:1422–1428.
- 94 Gould KL, Pan T, Loghini C, Johnson NP, Guha A, Sdringola S. Frequent diagnostic errors in cardiac PET/CT due to misregistration of CT attenuation and emission PET images: a definitive analysis of causes, consequences, and corrections. *J Nucl Med* 2007; **48**:1112–1121.
- 95 Goetze S, Brown TL, Lavelly WC, Zhang Z, Bengel FM. Attenuation correction in myocardial perfusion SPECT/CT: effects of misregistration and value of reregistration. *J Nucl Med* 2007; **48**:1090–1095.
- 96 Sourbelle K, Kachelriess M, Kalender WA. Reconstruction from truncated projections in CT using adaptive detruncation. *Eur Radiol* 2005; **15**:1008–1014.
- 97 Michel C, Noo F, Sibomana M, Faul D. An iterative method for creating attenuation maps from highly truncated CT data. In: Noo F, Kudo H, Zeng L, editors. Proc of the VIIIth International Meeting on Fully Three-dimensional Image Reconstruction in Radiology and Nuclear Medicine, 6–9 July 2005, Salt Lake City, Utah, USA; 2005. Available online at http://www.fully3d.org/2005/3D05_proceedings.pdf.
- 98 Mawlawi O, Erasmus JJ, Pan T, Cody Dd, Campbell R, Lonn AH, et al. Truncation artifact on PET/CT: impact on measurements of activity concentration and assessment of a correction algorithm. *AJR Am J Roentgenol* 2006; **186**:1458–1467.
- 99 Beyer T, Bockisch A, Kuhl H, Martinez MJ. Whole-body 18F-FDG PET/CT in the presence of truncation artifacts. *J Nucl Med* 2006; **47**:91–99.
- 100 Antoch G, Freudenberg LS, Egelhof T, Stattaus J, Jentzen W, Debatin JF, et al. Focal tracer uptake: a potential artifact in contrast-enhanced dual-modality PET/CT scans. *J Nucl Med* 2002; **43**:1339–1342.
- 101 Antoch G, Freudenberg LS, Beyer T, Bockisch A, Debatin JF. To enhance or not to enhance? 18F-FDG and CT contrast agents in dual-modality 18F-FDG PET/CT. *J Nucl Med* 2004; **45**(suppl 1):56S–65S.
- 102 Antoch G, Kuehl H, Kanja J, Lauenstein TC, Schneemann H, Hauth E, et al. Dual-modality PET/CT scanning with negative oral contrast agent to avoid artifacts: introduction and evaluation. *Radiology* 2004; **230**:879–885.
- 103 Dizendorf EV, Treyer V, Von Schulthess GK, Hany TF. Application of oral contrast media in coregistered positron emission tomography-CT. *AJR Am J Roentgenol* 2002; **179**:477–481.
- 104 Nehmeh SA, Erdi YE, Kalaigian H, Kolbert KS, Pan T, Yeung H, et al. Correction for oral contrast artifacts in CT attenuation-corrected PET images obtained by combined PET/CT. *J Nucl Med* 2003; **44**:1940–1944.
- 105 Nakamoto Y, Chin BB, Kraitchman DL, Lawler LP, Marshall LT, Wahl RL. Effects of nonionic intravenous contrast agents in PET/CT imaging: phantom and canine studies. *Radiology* 2003; **227**:817–824.

- 106 Yau Y-Y, Chan W-S, Tam Y-M, Vernon P, Wong S, Coel M, *et al.* Application of intravenous contrast in PET/CT: does it really introduce significant attenuation correction error? *J Nucl Med* 2005; **46**:283–291.
- 107 Dizendorf E, Hany TF, Buck A, von Schulthess GK, Burger C. Cause and magnitude of the error induced by oral CT contrast agent in CT-based attenuation correction of PET emission studies. *J Nucl Med* 2003; **44**:732–738.
- 108 Berthelsen AK, Holm S, Loft A, Klausen TL, Andersen F, Hojgaard L. PET/CT with intravenous contrast can be used for PET attenuation correction in cancer patients. *Eur J Nucl Med Mol Imaging* 2005; **32**:1167–1175.
- 109 Groves AM, Kayani I, Dickson JC, Townsend C, Croasdale I, Syed R, *et al.* Oral contrast medium in PET/CT: should you or shouldn't you? *Eur J Nucl Med Mol Imaging* 2005; **32**:1160–1166.
- 110 Beyer T, Antoch G, Bockisch A, Stattaus J. Optimized intravenous contrast administration for diagnostic whole-body 18F-FDG PET/CT. *J Nucl Med* 2005; **46**:429–435.
- 111 Heiba SI, Luo J, Sadek S, Macalental E, Cacavio A, Rosen G, *et al.* Attenuation-correction induced artifact in F-18 FDG PET imaging following total knee replacement. *Clin Positron Imaging* 2000; **3**:237–239.
- 112 Halpern BS, Dahlbom M, Waldherr C, Yap CS, Schiepers C, Silverman DH, *et al.* Cardiac pacemakers and central venous lines can induce focal artifacts on CT-corrected PET images. *J Nucl Med* 2004; **45**:290–293.
- 113 DiFilippo FP, Brunken RC. Do implanted pacemaker leads and ICD leads cause metal-related artifact in cardiac PET/CT? *J Nucl Med* 2005; **46**:436–443.
- 114 Goerres GW, Hany TF, Kamel E, von Schulthess GK, Buck A. Head and neck imaging with PET and PET/CT: artefacts from dental metallic implants. *Eur J Nucl Med Mol Imaging* 2002; **29**:367–370.
- 115 Goerres GW, Ziegler SI, Burger C, Berthold T, Von Schulthess GK, Buck A. Artifacts at PET and PET/CT caused by metallic hip prosthetic material. *Radiology* 2003; **226**:577–584.
- 116 Kamel EM, Burger C, Buck A, von Schulthess GK, Goerres GW. Impact of metallic dental implants on CT-based attenuation correction in a combined PET/CT scanner. *Eur Radiol* 2003; **13**:724–728.
- 117 Bujenovic S, Mannting F, Chakrabarti R, Ladrner D. Artifactual 2-deoxy-2-[(18)F]fluoro-D-glucose localization surrounding metallic objects in a PET/CT scanner using CT-based attenuation correction. *Mol Imaging Biol* 2003; **5**:20–22.
- 118 Hsieh J, Molthen RC, Dawson CA, Johnson RH. An iterative approach to the beam hardening correction in cone beam CT. *Med Phys* 2000; **27**:23–29.
- 119 Kachelriebe M, Kalender WA. Improving PET/CT attenuation correction with iterative CT beam hardening correction. *IEEE Nuclear Science Symposium Conference Record* 2005; **4**:5.
- 120 Ay M, Zaidi H. Assessment of errors caused by x-ray scatter and use of contrast medium when using CT-based attenuation correction in PET. *Eur J Nucl Med Mol Imaging* 2006; **33**:1301–1313.
- 121 Zbijewski W, Beekman FJ. Efficient Monte Carlo based scatter artifact reduction in cone-beam micro-CT. *IEEE Trans Med Imaging* 2006; **25**:817–827.
- 122 Siewerdsen JH, Daly MJ, Bakhtiar B, Moseley DJ, Richard S, Keller H, *et al.* A simple, direct method for x-ray scatter estimation and correction in digital radiography and cone-beam CT. *Med Phys* 2006; **33**:187–197.
- 123 Chang LT. A method for attenuation correction in radionuclide computed tomography. *IEEE Trans Nucl Sci* 1978; **25**:638–643.
- 124 Gullberg GT, Huesman RH, Malko JA, Pelc NJ, Budinger TF. An attenuated projector-backprojector for iterative SPECT reconstruction. *Phys Med Biol* 1985; **30**:799–816.
- 125 Li Q, Leahy RM. Statistical modeling and reconstruction of randoms precorrected PET data. *IEEE Trans Med Imaging* 2006; **25**:1565–1572.
- 126 Rokitta O, Casey M, Wienhard K, Picrzyk U. Random correction for positron emission tomography using singles count rates. *IEEE Nuclear Science Symposium Conference Record* 2000; **3**:37–40.
- 127 Casey M, Hoffman E. Quantitation in positron emission tomography: 7. A technique to reduce noise in accidental coincidence measurements and coincidence efficiency calibration. *J Comput Assist Tomogr* 1986; **10**:845–850.
- 128 Mumcuoglu EU, Leahy RM, Cherry SR. Bayesian reconstruction of PET images: methodology and performance analysis. *Phys Med Biol* 1996; **41**:1777–1807.
- 129 Badawi R, Miller M, Bailey D, Marsden P. Randoms variance-reduction in 3D-PET. *Phys Med Biol* 1999; **44**:941–954.
- 130 Zaidi H. Recent developments and future trends in nuclear medicine instrumentation. *Z Med Phys* 2006; **16**:5–17.
- 131 Derenzo SE, Weber MJ, Bourret-Courchesne E, Klintonberg MK. The quest for the ideal inorganic scintillator. *Nucl Instr Meth A* 2003; **505**:111–117.
- 132 Moses WW. Time of flight in PET revisited. *IEEE Trans Nucl Sci* 2003; **50**:1325–1330.
- 133 Ter-Pogossian MM, Mullani NA, Ficke DC, Markham J, Snyder DL. Photon time-of-flight-assisted positron emission tomography. *J Comput Assist Tomogr* 1981; **5**:227–239.
- 134 Tomitani T. Image reconstruction and noise evaluation in photon time-of-flight assisted positron emission tomography. *IEEE Trans Nucl Sci* 1981; **28**:4582–4589.
- 135 Conti M, Bendriem B, Casey M, Chen M, Kehren F, Michel C, *et al.* First experimental results of time-of-flight reconstruction on an LSO PET scanner. *Phys Med Biol* 2005; **50**:4507–4526.
- 136 Moszynski M, Kapusta M, Nassalski A, Szczesniak T, Wolsik D, Eriksson L, *et al.* New prospects for time-of-flight PET with LSO scintillators. *IEEE Trans Nucl Sci* 2006; **53**:2484–2488.
- 137 Surti S, Kuhn A, Werner ME, Perkins AE, Kolthammer J, Karp JS. Performance of Philips Gemini TF PET/CT scanner with special consideration for its time-of-flight imaging capabilities. *J Nucl Med* 2007; **48**:471–480.
- 138 Conti M. Effect of randoms on signal-to-noise ratio in TOF PET. *IEEE Trans Nucl Sci* 2006; **53**:1188–1193.
- 139 Wang W, Tsui B, Balush D, Tocharoenchai C, Frey E. Optimization of acquisition parameters for simultaneous ²⁰¹Tl and ^{99m}Tc dual-isotope myocardial imaging. *IEEE Trans Nucl Sci* 2005; **52**:1227–1235.
- 140 Du Y, Frey E, Wang W, Tsui B. Optimization of acquisition energy windows in simultaneous ^{99m}Tc/¹²³I brain SPECT. *IEEE Trans Nucl Sci* 2003; **50**:1556–1561.
- 141 de Jong HW, Beekman FJ, Viergever MA, van Rijk PP. Simultaneous (99m)Tc/(201)Tl dual-isotope SPET with Monte Carlo-based down-scatter correction. *Eur J Nucl Med Mol Imaging* 2002; **29**:1063–1071.
- 142 Song X, Frey E, Wang W, Du Y, Tsui B. Validation and evaluation of model based crosstalk compensation method in simultaneous ^{99m}Tc stress and ²⁰¹Tl rest myocardial perfusion SPECT. *IEEE Trans Nucl Sci* 2004; **51**:72–79.
- 143 Ouyang J, Fakhri GE, Moore SC. Fast Monte Carlo based joint iterative reconstruction for simultaneous ^{99m}Tc/¹²³I SPECT imaging. *Med Phys* 2007; **34**:3263–3272.
- 144 Kadmas DJ, Rust TC. Feasibility of rapid multitracer PET tumor imaging. *IEEE Trans Nucl Sci* 2005; **52**:1341–1347.
- 145 Rust TC, Kadmas DJ. Rapid dual-tracer PTSM + ATSM PET imaging of tumour blood flow and hypoxia: a simulation study. *Phys Med Biol* 2006; **51**:61–75.
- 146 Rust TC, DiBella EVR, McGann CJ, Christian PE, Hoffman JM, Kadmas DJ. Rapid dual-injection single-scan ¹³N-ammonia PET for quantification of rest and stress myocardial blood flows. *Phys Med Biol* 2006; **51**:5347–5362.
- 147 Verhaeghe J, D'Asseler Y, Staelens S, Lemahieu I. Noise properties of simultaneous dual tracer PET imaging. *IEEE Nuclear Science Symposium Conference Record* 2005; **5**:2611–2614.
- 148 El Fakhri G, Sitek A, Guérin B. Simultaneous dual tracer PET using generalized factor analysis of dynamic sequences. *IEEE Nuclear Science Symposium Conference Record* 2006; **4**:2128–2130.
- 149 Zaidi H, Koral KF. Scatter modelling and compensation in emission tomography. *Eur J Nucl Med Mol Imaging* 2004; **31**:761–782.
- 150 Soret M, Bacharach SL, Buvat I. Partial-volume effect in PET tumor imaging. *J Nucl Med* 2007; **48**:932–945.
- 151 Rousset OG, Rahmim A, Alavi A, Zaidi H. Partial volume correction strategies in PET. *PET Clinics* 2007; **2**:(in press).
- 152 Frey EC, Tsui BMW. A fast projector-backprojector pair modeling the asymmetric, spatially varying scatter response function for scatter compensation in SPECT imaging. *IEEE Trans Nucl Sci* 1993; **40**:1192–1197.
- 153 Beekman FJ, de Jong HW, Slijpen ET. Efficient SPECT scatter calculation in non-uniform media using correlated Monte Carlo simulation. *Phys Med Biol* 1999; **44**:N183–N192.
- 154 Werling A, Bublitz O, Doll J, Adam LE, Brix G. Fast implementation of the single scatter simulation algorithm and its use in iterative image reconstruction of PET data. *Phys Med Biol* 2002; **47**:2947–2960.
- 155 Vandervoort E, Celler A, Wells G, Blinder S, Dixon K, Pang Y. Implementation of an analytically based scatter correction in SPECT reconstructions. *IEEE Trans Nucl Sci* 2005; **52**:645–653.
- 156 Tamal M, Reader AJ, Markiewicz PJ, Julyan PJ, Hastings DL. Noise properties of four strategies for incorporation of scatter and attenuation information in PET reconstruction using the EM-ML algorithm. *IEEE Trans Nucl Sci* 2006; **53**:2778–2786.
- 157 Beekman FJ, de Jong HW, van Geloven S. Efficient fully 3-D iterative SPECT reconstruction with Monte Carlo-based scatter compensation. *IEEE Trans Med Imaging* 2002; **21**:867–877.

- 158 Lazaro D, El Bitar Z, Breton V, Hill D, Buvat I. Fully 3D Monte Carlo reconstruction in SPECT: a feasibility study. *Phys Med Biol* 2005; **50**:3739–3754.
- 159 Cot A, Falcon C, Crespo C, Sempau J, Pareto D, Bullich S, *et al.* Absolute quantification in dopaminergic neurotransmission SPECT using a Monte Carlo-based scatter correction and fully 3-dimensional reconstruction. *J Nucl Med* 2005; **46**:1497–1504.
- 160 Dewaraja YK, Ljungberg M, Fessler JA. 3-D Monte Carlo-based scatter compensation in quantitative I-131 SPECT reconstruction. *IEEE Trans Nucl Sci* 2006; **53**:181–188.
- 161 Rehfeld N, Alber M. A parallelizable compression scheme for Monte Carlo scatter system matrices in PET image reconstruction. *Phys Med Biol* 2007; **52**:3421–3437.
- 162 Tellmann L, Fulton R, Pietrzyk U, Nickel I, Stangier I, Winz O, *et al.* Concepts of registration and correction of head motion in positron emission tomography. *Z Med Phys* 2006; **16**:67–74.
- 163 Lu W, Mackie TR. Tomographic motion detection and correction directly in sinogram space. *Phys Med Biol* 2002; **47**:1267–1284.
- 164 Beekman F, Hutton B. Multi-modality imaging on track. *Eur J Nuc Med Mol Imaging* 2007; **34**:1410–1414.